

Article

# Using Geospatial Analysis and Hydrologic Modeling to Estimate Climate Change Impacts on Nitrogen Export: Case Study for a Forest and Pasture Dominated Watershed in North Carolina

Md Jahangir Alam <sup>1</sup>, Mehmet B. Ercan <sup>2</sup>, Faria Tuz Zahura <sup>3</sup>  and Jonathan L. Goodall <sup>3,\*</sup> 

<sup>1</sup> Hazen and Sawyer, Birmingham, AL 35244, USA; malam@hazenandsawyer.com

<sup>2</sup> Department of Civil Engineering, Inonu University, Malatya 44280, Turkey; mehmetbercan@gmail.com

<sup>3</sup> Department of Civil and Environmental Engineering, University of Virginia, Charlottesville, VA 22903, USA; fz7xb@virginia.edu

\* Correspondence: goodall@virginia.edu; Tel.: +1-(434)-243-5019

Received: 31 May 2018; Accepted: 20 July 2018; Published: 21 July 2018



**Abstract:** Many watersheds are currently experiencing streamflow and water quality related problems that are caused by excess nitrogen. Given that weather is a major driver of nitrogen transport through watersheds, the objective of this study was to predict climate change impacts on streamflow and nitrogen export. A forest and pasture dominated watershed in North Carolina Piedmont region was used as the study area. A physically-based Soil and Water Assessment Tool (SWAT) model parameterized using geospatial data layers and spatially downscaled temperature and precipitation estimates from eight different General Circulation Models (GCMs) were used for this study. While temperature change predictions are fairly consistent across the GCMs for the study watershed, there is significant variability in precipitation change predictions across the GCMs, and this leads to uncertainty in the future conditions within the watershed. However, when the downscaled GCM projections were taken as a model ensemble, the results suggest that both high and low emission scenarios would result in an average increase in streamflow of 14.1% and 12.5%, respectively, and a decrease in the inorganic nitrogen export by 12.1% and 8.5%, respectively, by the end of the century. The results also show clear seasonal patterns with streamflow and nitrogen loading both increasing in fall and winter months by 97.8% and 50.8%, respectively, and decreasing by 20.2% and 35.5%, respectively, in spring and summer months by the end of the century.

**Keywords:** climate change; nitrogen; environmental modeling; SWAT; GIS

## 1. Introduction

Adverse effects of climate change in global natural systems are well-documented by the Intergovernmental Panel on Climate Change [1], and studies have shown that future climate change will alter the watershed hydrologic processes and nutrient transport characteristics across the globe [2]. Historical trend data demonstrates the climate change impacts throughout the United States [3]. Studies suggest that future climate change will impact terrestrial and aquatic ecosystems on various spatial and temporal scales [1]. Climate change can introduce significant stress on the sustainability of the agriculture, forestry, fisheries, and water supply systems [1,4]. Studies on surface water quality suggest that climate change may increase nonpoint source pollution loads in North America [5]. For these reasons, assessing climate change impacts on watershed systems is important to develop alternative strategies and policies to mitigate its adverse effects.

During the latter half of the twentieth century, anthropogenic activities have doubled the reactive nitrogen in the environment [6]. This excess fixed nitrogen in the environment is responsible for severe water quality degradation, loss in biodiversity, and serious human health risks [6]. Future climate change will significantly alter the nitrogen cycle and it may exacerbate nitrogen pollution [2]. Moreover, watersheds with water scarcity will likely worsen problems of elevated fixed nitrogen [7]. Climate change is expected to increase algal blooms that are associated with nutrient and warm water [8]. In the contiguous United States, eutrophication has already caused severe degradation for 40% and moderate to severe degradation for 67% of estuarine areas [9]. Harmful algal blooms can cause destruction in the marine food web structure [10].

To investigate future climate impacts, general circulation models (GCMs) are often used, but GCM output resolutions are spatially coarse presenting challenges for many hydrological and ecological studies [11]. Various spatial downscaling approaches can be used to obtain finer resolution climate projections from GCMs. The downscaled climate data can be used as an input to physically-based hydrologic models to better understand potential climate change impacts on water quantity and quality. The Soil and Water Assessment Tool (SWAT) [12] is a widely used watershed-scale hydrologic model that has been successfully applied for many hydrologic and water quality studies around the globe. Geographic Information System (GIS) extensions, such as ArcSWAT, can be used to bridge the gap between geospatial data layers, such as soil maps, land use maps, spatially variable temperature and precipitation estimates, and the hydrologic model simulation engine [13]. These tools make use of geoprocessing algorithms to summarize datasets into key model parameters and other input files that are required by the model [13]. We used ArcSWAT and our own custom geoprocessing algorithms in this study to incorporate the downscaled GCM data into the hydrologic model.

The Eno River was selected as the study watershed because it is an important water source for a growing community within the Research Triangle Park region of North Carolina, USA. The watershed is dominated by forest and pasture lands and has gone through aggressive preservation efforts. The objective of this study is to use geospatial analysis and hydrologic modeling to better understand the potential climate change impacts on streamflow and water quality in the study region and other watersheds with similar watershed characteristics and future climate projections. As many studies suggest, multiple GCMs and emission scenarios are needed to capture the range of future projections [14–17]. Therefore, an ensemble of eight GCMs for two different emission scenarios is used for future climate projections. These GCM outputs are used to drive a calibrated SWAT model to simulate streamflow and inorganic nitrogen export. This study contributes to the growing research of climate change impacts in watershed hydrologic systems and water quality, specifically, on nitrogen export from watersheds with similar characteristics to the study watershed [18–23]. This study also contributes a methodology leveraging spatially-explicit data and analyses that can be applied to other critical and impaired watersheds across the world to better understand, from a mechanistic perspective, the specific relationship between changes in climate and nitrogen export for that watershed.

## 2. Materials and Methods

### 2.1. Study Area

The Eno River is a forest and pasture dominated watershed in North Carolina's Piedmont region with a drainage area of 364 sq km (Figure 1). This watershed has gently rolling topography and a mild, four-season climate. After running nearly 33 miles, the Eno River joins the Flat River to become the Neuse and it flows into Falls Lake. Due to water quality issues, the state of North Carolina declared the Falls Lake as an "impaired" waterbody. Deteriorated water quality with frequent algal blooms, hypoxic conditions, and fish kills brought the Neuse River to the national spotlight and has resulted in the river frequently being placed on the most "endangered rivers" watch list by the national conservation organization "American Rivers". The water quality issues in downstream Neuse was a motivating

factor for investigating the potential impact of future climate change on streamflow and nitrogen export in one of the key tributaries to the Neuse, the Eno River.

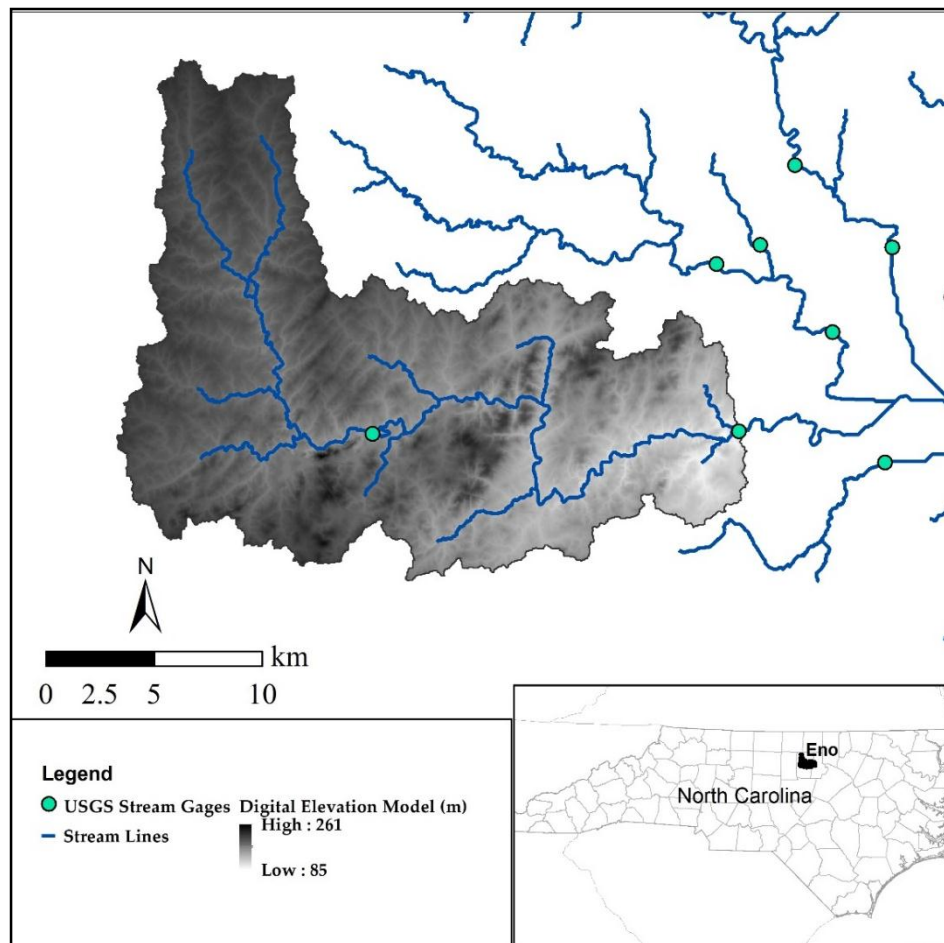


**Figure 1.** Eno River watershed study area, which is located in the North Carolina Piedmont region, showing the United States Geological Survey (USGS) monitoring stations.

## 2.2. Data Preparation

Digital elevation data (1031 columns and 850 rows) were obtained for the study region from the United States Geological Survey (USGS) 30 m resolution National Elevation Dataset (NED) [24]. According to the NED, elevation in the Eno watershed ranges from 85 to 261 m, with an average elevation of 199 m. The slope of the watershed ranges from 0 to 155%, with an average slope of 6.1%. The National Hydrography Dataset (NHD) and the NED were used to delineate the watershed boundaries in ArcGIS. Land cover data were obtained from the 30-m resolution 2006 version of the National Land Cover Dataset (NLCD) [25]. The 2006 version was used because the model calibration was done around that time period. According to the NLCD data, the watershed is dominated by forest (56%), pasture lands (26%), and developed area (mostly open space development) (11%) (Figure 2). Cultivated crops, grassland, scrub, and open water only each cover 2% of the watershed. Soil data was obtained from the United States Department of Agriculture (USDA) State Soil Geographic (STATSGO) dataset. According to the STATSGO dataset, the dominant soil types in the watershed are silty loam and sandy loam, and the hydrologic soil groups are mainly B but also C and D (Figure 2). At the time of the model development, the higher resolution Soil Survey Geographic Database (SSURGO) was not available in a spatially-explicit form for the entire watershed.

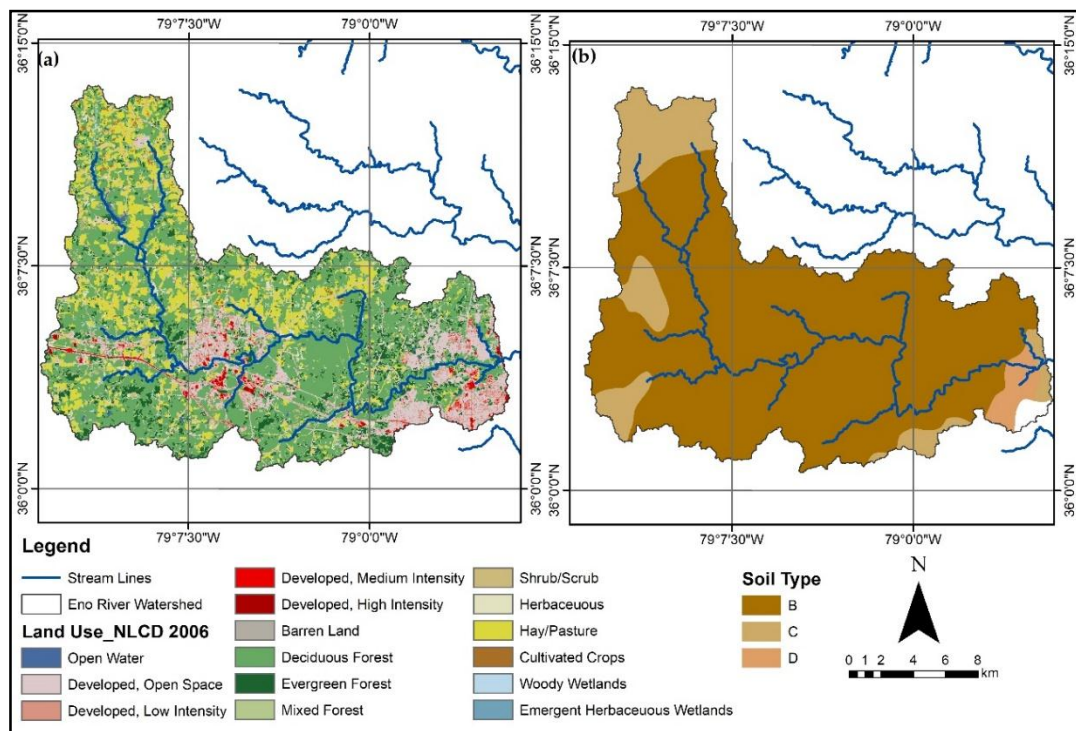


**Figure 2.** (a) National Land Cover Dataset (NLCD) 2006 land use and (b) State Soil Geographic (STATSGO) soil hydrologic groups within Eno River watershed study area. The grid represents  $1/8^\circ$  cells, showing the spatial resolution of the downscaled climate data.

Historic maximum and minimum air temperature, wind speed, and humidity data were obtained from the National Climatic Data Center (NCDC) for the SWAT calibration and validation simulation period of 2005–2010. Solar radiation was generated by the SWAT built-in weather generator [26]. Using the approach that was described by [27], composite watershed area-averaged precipitation data was derived from Nexrad-derived radar rainfall from the National Weather Service (NWS) and gauge observed rainfall from NCDC. Finally, observed daily streamflow and inorganic nitrogen concentration data were obtained from the USGS and EPA, who maintain monitoring stations on the Eno River near Durham, North Carolina. In this study, we defined “inorganic nitrogen” as “nitrate and nitrite as N” for nitrogen concentration measurements. A regression model Load Estimator (LOADEST), which is a program for estimating constituent loads in streams and rivers, was used to predict the continuous daily nitrogen loading from continuous daily observed streamflow and irregularly measured (approximately every two weeks) nitrogen concentration data [28].

### 2.3. Soil and Water Assessment Tool (SWAT) Model Setup

The Soil and Water Assessment Tool (SWAT) is a semi-distributed, physically-based model, which was developed by US Department of Agriculture (USDA) Agricultural Research Services (ARS) [12]. SWAT is well known for watershed-scale hydrologic and water quality modeling and is capable of long term, continuous, daily, and sub-daily time step modeling [29]. SWAT has been used to assess the impact of climate change, land use change, nonpoint source pollution, and different management practices on watershed hydrology and water quality modeling [12]. The United States Environmental Protection Agency (EPA) recommends SWAT for long term modeling of watersheds with mixed to complex land uses [30].

SWAT divides the watershed into multiple sub-watersheds, which are further divided into Hydrologic Response Units (HRUs). Each HRU represents a unique combination of soil, land use, and management practices and they are not spatially connected to each other but directly routed to the

outlet of the sub-watershed. The sub-watersheds are spatially defined and routed to the downstream sub-watershed. Each HRU contains surface runoff, lateral flow, and base flow components for in-stream discharge. The Eno River watershed was divided into 22 sub-watersheds and 200 HRUs that are based on streamflow location and watershed characteristics. A threshold value of 10% for soil, slope, and land cover was used to create HRUs within the sub-watersheds. The ArcSWAT interface, an ArcGIS extension that is mentioned in the Introduction section, was used to create the sub-watersheds and HRUs.

The USDA Natural Resources Conservation Service (NRCS) Curve Number (CN) method, formerly known as the Soil Conservation Service or SCS Runoff Curve Number, was used for surface runoff estimation [31]. Curve Number (CN) depends on soil type, land use, and hydrologic condition. Potential evapotranspiration (PET) was calculated using the Penman-Monteith method [32] that depends on solar radiation, air temperature, relative humidity, and wind speed. Finally, in-stream water and nitrogen routing were calculated using the variable storage routing method [33]. Model simulations are first done in each HRU and are then lumped to the sub-catchment scale. Sub-catchment water and nutrient content are then summed before being routed to the stream.

SWAT can simulate nitrogen movement and transformation in a soil profile and shallow aquifer. Typically, organic-N and nitrate stay dissolved in water or attached to the sediment and transported with the surface runoff, lateral flow, and percolation. SWAT can simulate nitrogen processes that include organic and inorganic fertilization, plant uptake, decomposition, mineralization, nitrification, denitrification, volatilization, atmospheric deposition, nitrogen rainfall, movement in water column, erosion, and leaching [12]. The organic-N transport model that was used in SWAT is based on equations developed by [34] and modified by [35]. SWAT estimates the denitrification rate as a function of water content, temperature, presence of a carbon source, and nitrate [36].

#### 2.4. Downscaled Future Climate Data

General Circulation Models (GCMs) are physically-based and are used to project changes in climate due to changes in environmental greenhouse gas concentration. To capture the variability in the projections, many studies recommend the use of multiple GCMs [14–17]. In this study, an ensemble of eight GCMs was used for the daily precipitation and temperature data for the base and future conditions (Table 1). All of the GCMs used for this work have been previously applied in various assessments of the Intergovernmental Panel on Climate Change (IPCC) Fourth Assessment Report [4]. GCMs that are used in this study are from the World Climate Research Programme's (WCRP's) Coupled Model Intercomparison Project Phase 3 (CMIP3) multimodel dataset [37]. While the CMIP5 dataset is now available, recent studies have shown that, compared to CMIP3, there are only small differences in magnitude and spatial distribution of model outputs, such as precipitation [38,39], which implies that the results for this study would be consistent with any results determined using CMIP5.

**Table 1.** The eight General Circulation Models (GCMs) that were used for precipitation and temperature projections.

Climate Models	Institutions, Sponsoring Agency, Country	References
CGCM3.1 (T47)	Canadian Centre for Climate Modeling & Analysis	[40]
CNRM-CM3	Météo-France/Centre National de Recherches Météorologiques, France	[41]
GFDL-CM2.1	US Dept. of Commerce/NOAA/Geophysical Fluid Dynamics Laboratory, USA	[42]
IPSL-CM4	Institut Pierre Simon Laplace, France	[43]
MIROC3.2 (medres)	Center for Climate System Research (The University of Tokyo), National Institute for Environmental Studies, Frontier Research Center for Global Change (JAMSTEC), Japan	[44]
ECHO-G	Meteorological Institute of the University of Bonn, Meteorological Research Institute of KMA	[45]
ECHAM5/MPI-OM	Max Planck Institute for Meteorology, Germany	[46]
MRI-CGCM2.3.2	Meteorological Research Institute, Japan	[47]

As the GCM data is available in coarse resolution, usually a few hundred kilometers [48], and is not suitable for the analysis of regional and local-scale hydrologic and biogeochemical processes, it was bias-corrected while using quantile-mapping approach and statistically downscaled to a  $1/8^\circ$  grid cell (approximately 12 by 12 km as shown in Figure 2) using interpolation of bias-corrected GCM anomalies on fine-scale grid of historical climate data as described by [17]. GCM outputs are available in different emission scenarios where each scenario represents a different assumption for future human activity, greenhouse gas emission, technology development, and economic growth. In this study, we used the high emissions scenario (A2) and the low emissions scenario (B1) to capture the range of possibilities.

In this study, spatially downscaled daily precipitation and temperature data for the time period 1961–2000, 2046–2065, 2081–2100 were obtained from the eight downscaled GCMs (Table 1). Custom geoprocessing scripts were created to feed the data into the calibrated SWAT model in order to estimate climate change impacts on streamflow and inorganic nitrogen loading in the Eno River. The first nine years of the simulation (1961–1969) were ignored in later analyses as these were considered to be a model warm-up period where initial conditions (e.g., soil moisture, streamflow, etc.) are established in the model. We defined the base conditions as 1970–2000, mid-century as 2048–2065, and end-century as 2085–2099 for reporting the study results.

Analyzing the downscaled temperature data shows that future projections for temperature are consistently higher for all time periods and emission scenarios (Table 2). For the A2 scenario, the maximum temperature is projected to increase between 1.7 to 3.0 °C and 3.3 to 5.6 °C by mid-century and end century, respectively, from the base period. For the B2 scenario, these increases are between 1.5 to 2.4 °C and 1.9 to 3.0 °C, respectively. Average minimum temperature will also increase between 1.7 to 2.7 °C by the mid-century and 3.4 to 5.2 °C by the end century for the A2 scenario. These increases are between 1.4 to 2.2 °C and 1.9 to 3.0 °C, respectively, for the B1 scenario. Future precipitation projections vary more widely from model to model (Table 2). While some of the GCMs predict an overall increase in precipitation, others predict a decrease. According to these models, precipitation in the A2 scenario will change anywhere between −14.7 to 12.5% and −21.3 to 13.3% by mid-century and end century, respectively, from the base period. For the B1 scenario, these precipitation changes are projected to be between −6.7 to 7.9% and −10.0 to 10.2% by mid-century and end century from the base period.

**Table 2.** Changes in daily average temperature (°C) and precipitation (%) over the next century as modeled by the eight GCMs used in this study [37].

Time Period <sup>a</sup>	Scenario	CGCM 3.1	CNRM-CM3	GFDL-CM2.1	IPSL-CM4	MIROC 3.2	ECHO-G	ECHAM5/MPI-OM	MRI-CGCM 2.3.2
<i>Change in Maximum Daily Temperature (°C)</i>									
Mid	A2	2.2	2.0	2.6	2.6	3.0	2.6	1.8	1.7
	B1	1.5	1.6	1.6	2.2	2.4	1.8	1.8	1.5
End	A2	3.9	4.4	4.7	4.7	5.6	4.1	4.0	3.3
	B1	2.0	2.2	2.0	2.9	3.0	2.7	2.7	1.9
<i>Change in Minimum Daily Temperature (°C)</i>									
Mid	A2	2.4	2.1	2.6	2.7	2.7	2.6	1.9	1.7
	B1	1.7	1.5	1.7	2.2	2.1	1.8	1.7	1.4
End	A2	4.4	4.3	4.8	5.2	5.2	4.5	4.4	3.4
	B1	2.2	2.0	2.1	3.0	2.8	2.7	2.9	1.9
<i>Change in Daily Precipitation (%)</i>									
Mid	A2	5.9	12.3	12.4	−12.2	−14.7	−1.9	12.5	2.6
	B1	1.0	1.4	7.9	−4.7	−6.7	4.5	5.7	1.9
End	A2	11.7	1.2	3.8	−13.6	−21.3	4.5	13.3	6.5
	B1	3.2	10.1	10.2	−10.0	−0.9	−4.1	8.1	−3.7

<sup>a</sup> 'Mid' and 'End' refer to mid-century (2048–2065) and end-century (2085–2099) time periods, respectively. Values refer to the change from the baseline period (1970–2000).

### 3. Results

#### 3.1. Model Calibration and Validation

The SWAT model was calibrated at the outlet of the watershed using the USGS streamflow data (USGS gauge 02085070) and inorganic nitrogen concentration data (EPA station J0770000). Before calibration, a sensitivity analysis was done to select parameters that were most sensitive to stream discharge and nitrogen loading. In this study, we used the Generalized Likelihood Uncertainty Estimation (GLUE) [49] method available in SWAT-CUP [50] to explore parameter sensitivity. Instead of individual parameters, GLUE focuses on parameter sets to determine the model performance. Based on this analysis, we determined the parameters for both streamflow and nitrogen that the model is most sensitive to. These parameters were the focus of the model calibration.

Multi-objective calibration algorithms can increase model performance for large watersheds [51]. As a part of multi-objective calibration, two objective functions, Nash-Sutcliffe ( $E$ ) and Percent Bias ( $PB$ ), were used in the calibration process. This study used Non-Dominated Sorting Genetic Algorithm II (NSGA-II), which is population-based, fast, and efficient in optimization [52]. The NSGA-II method was implemented using a Python tool developed by [53]. The SWAT model was calibrated at a daily time step for the period 2005–2008, validated for the period 2009–2010 with a model warm-up period of 2002–2004 for both the streamflow and inorganic nitrogen.

The Nash-Sutcliffe coefficient of efficiency ( $E$ ), Logarithmic Nash-Sutcliffe ( $LogE$ ), coefficient of determination ( $R^2$ ), and Percent Bias ( $PB$ ) were used to evaluate the accuracy of the predicted values of streamflow and nitrogen export [36].  $E$  values range from  $-\infty$  to 1, where an  $E$  value of 1 represents the perfect prediction of the observed data. As the  $E$  values are based on squared differences and they are sensitive to extreme/peak values,  $LogE$  values were also estimated. The  $LogE$  value is more sensitive to the low values and it indicates how well the model matches to the observed data, especially for the low values. The  $R^2$  values range from 0 to 1, with 1 representing a perfect fit between modeled and observed values. Finally, Percent Bias ( $PB$ ) was calculated where a negative Percent Bias ( $PB$ ) indicates an overestimation in predictions and a positive Percent Bias ( $PB$ ) indicates an underestimation in predictions.

The performance metrics for streamflow estimation during the calibration period were  $E = 0.78$ ,  $LogE = 0.75$ ,  $R^2 = 0.78$ , and  $PB = -1.3$ . Using this calibrated model and applying the model to the validation period, the streamflow prediction performance metrics were  $E = 0.64$ ,  $LogE = 0.77$ ,  $R^2 = 0.65$ , and  $PB = -22.03$  (Figure 3). According to established best practices for SWAT modeling [54], this is a satisfactory model result for the validation period because  $E > 0.5$  and  $PB$  is  $\pm 25$ . The inorganic nitrogen performance metrics were  $E = 0.32$ ,  $LogE = 0.66$ ,  $R^2 = 0.37$ , and  $PB = 33.9$  for the calibration period and  $E = 0.36$ ,  $LogE = 0.73$ ,  $R^2 = 0.41$ , and  $PB = 0.37$  for the validation period (Figure 4).  $PB \pm 70$  for nitrogen calibration is considered to be satisfactory according to [54], however we acknowledge the limitation of the nitrogen calibration, which is in part due to infrequently measured nitrogen concentration data within the study watershed (and many other watersheds beyond dedicated experimental watersheds with long term observational records).

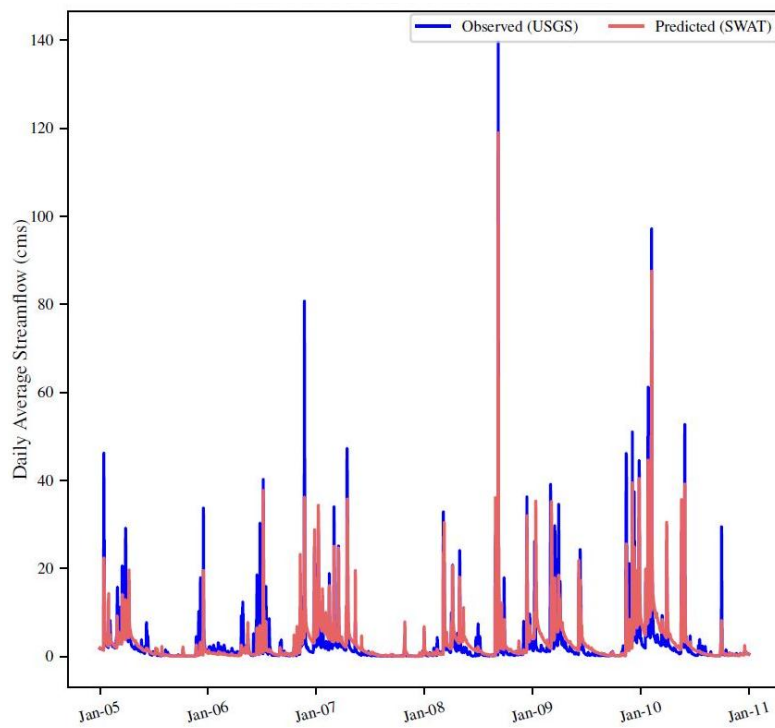


**Figure 3.** Comparison of observed daily streamflow at the USGS station 02085070 with Soil and Water Assessment Tool (SWAT) simulated daily streamflow.

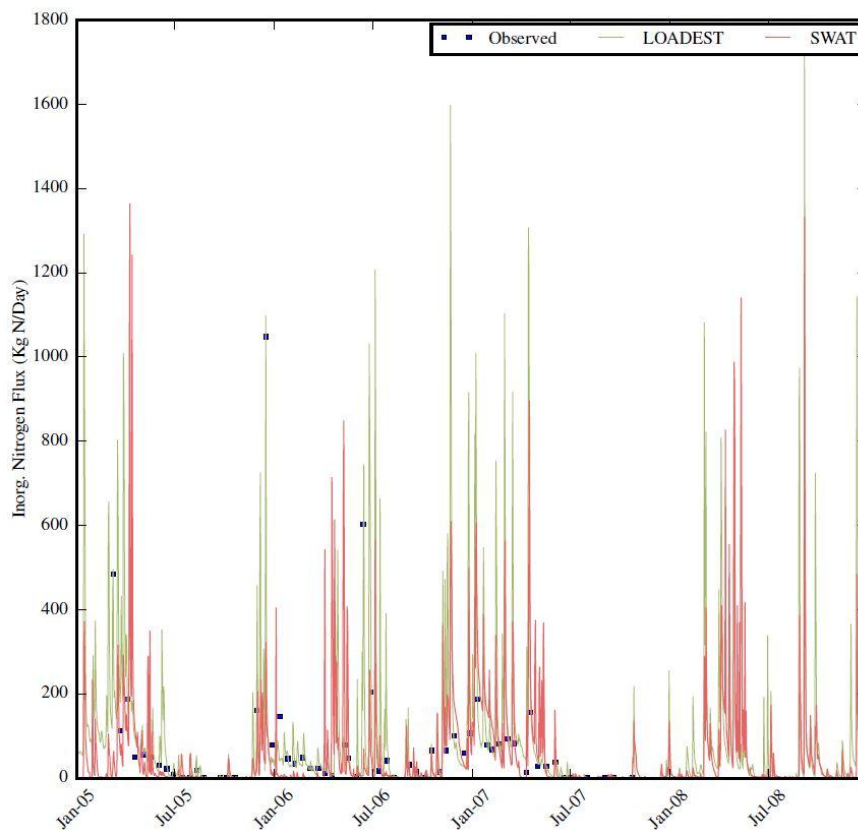


**Figure 4.** Comparison of observed daily inorganic nitrogen load at the Environmental Protection Agency (EPA) station J0770000 with LOADEST and SWAT simulated inorganic nitrogen load.

### 3.2. Projected Changes in Streamflow

The ensemble SWAT model simulations with the eight GCM outputs predict increases in daily average streamflow over the century for both the A2 and B1 scenarios. This is in part due to the fact that the ensemble average of the eight climate models for both A2 and B1 scenarios estimate small increases (average 1.3% by 2050) in precipitation. For the A2 scenario, the results estimate daily average streamflow increase of 13.7% (59.6 to −29.9%) by mid-century (2048–2065) and 14.1% (58.0 to −38.0%) by end century (2085–2099) from the base period streamflow ( $2.69 \text{ m}^3\text{s}^{-1}$ ) across the models. For the B1 scenario, these increases are 9.1% (35.3 to −5.3%) and 12.5% (43.3 to −21.8%), respectively.

As expected, the SWAT results showed a wider range of monthly average streamflow values for the A2 scenario than the B1 scenario (Figures 5 and 6 and Table 3). The variability in streamflow estimations can be explained by the significant variability in the precipitation projection across the eight models (Table 2). While both the A2 and B1 scenario estimate an overall increase in streamflow, perhaps being more significant are the estimated seasonal changes in streamflow projected by the model. For both the A2 and B1 scenarios, the models are in agreement that there will be an average increase in streamflow in winter and fall months across the models of 97.8% with a range between 38.5 to 189.4% by the end century (Table 4). On the other hand, streamflow decrease will be seen in spring and summer months for both the A2 and B1 scenarios by −20.2% (−2.4 to −40.3%) by the end century.

**Table 3.** Simulated changes in streamflow (%) and inorganic nitrogen loading (%) under future climate scenarios from the eight GCMs used in this study [37].

Time Period <sup>a</sup>	Scenario	CGCM 3.1	CNRM-CM3	GFDL-CM2.1	IPSL-CM4	MIROC 3.2	ECHO-G	ECHAM5/MPI-OM	MRI-CGCM 2.3.2
<i>Change in Streamflow (%)</i>									
Mid	A2	21.8	34.8	59.6	−29.9	−25.2	−5.5	45.2	19.0
	B1	−2.5	2.2	35.3	−4.2	−5.3	9.3	31.2	11.2
End	A2	37.2	13.4	39.3	−35.4	−38.0	12.1	58.0	29.5
	B1	10.2	35.5	43.3	−21.8	14.4	−6.6	33.5	0.1
<i>Change in Inorganic Nitrogen Loading (%)</i>									
Mid	A2	12.0	28.6	34.6	−44.9	−40.5	−36.2	33.5	0.7
	B1	−17.0	−11.5	11.4	−23.3	−12.1	−25.5	23.0	−14.3
End	A2	15.9	−9.9	9.8	−53.4	−51.1	−27.1	25.2	−1.9
	B1	−11.1	4.4	24.4	−20.1	2.4	−32.5	3.1	−26.6

<sup>a</sup> ‘Mid’ and ‘End’ refer to mid-century (2048–2065) and end-century (2085–2099) time periods, respectively. Values refer to the change from the baseline period (1970–2000).

**Table 4.** Seasonal percent changes in streamflow and inorganic nitrogen loading by mid-century (2048–2065) and end-century (2085–2099) from the base period for different emission scenarios. Values refer to the change from baseline period (1970–2000).

Climate Scenario	Period	Winter	Spring	Summer	Fall
<i>Percent change in streamflow</i>					
A2	Mid Century	42.21	−1.43	−24.85	95.83
A2	End Century	55.60	−12.79	−40.32	189.43
B1	Mid Century	28.28	−0.53	−26.35	82.58
B1	End Century	38.53	−2.39	−25.39	107.70
<i>Percent change in inorganic Nitrogen</i>					
A2	Mid Century	20.52	−14.71	−31.95	59.38
A2	End Century	21.38	−29.60	−48.74	107.81
B1	Mid Century	8.84	−18.32	−39.60	49.57
B1	End Century	10.66	−17.8	−45.79	63.16

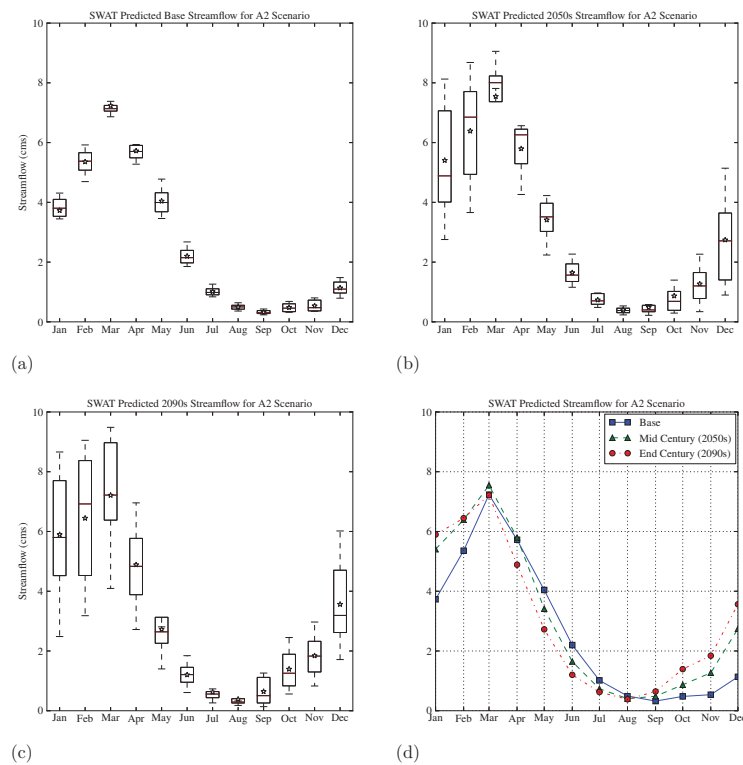


**Figure 5.** SWAT predicted monthly average streamflow. (a) Base period (1970–2000); (b) Mid–Century (2048–2065); (c) End–Century (2085–2099); from 8 GCMs predicted A2 emission scenarios at USGS station 02085070; (d) the average streamflow over the 8 GCMs for the three study periods.

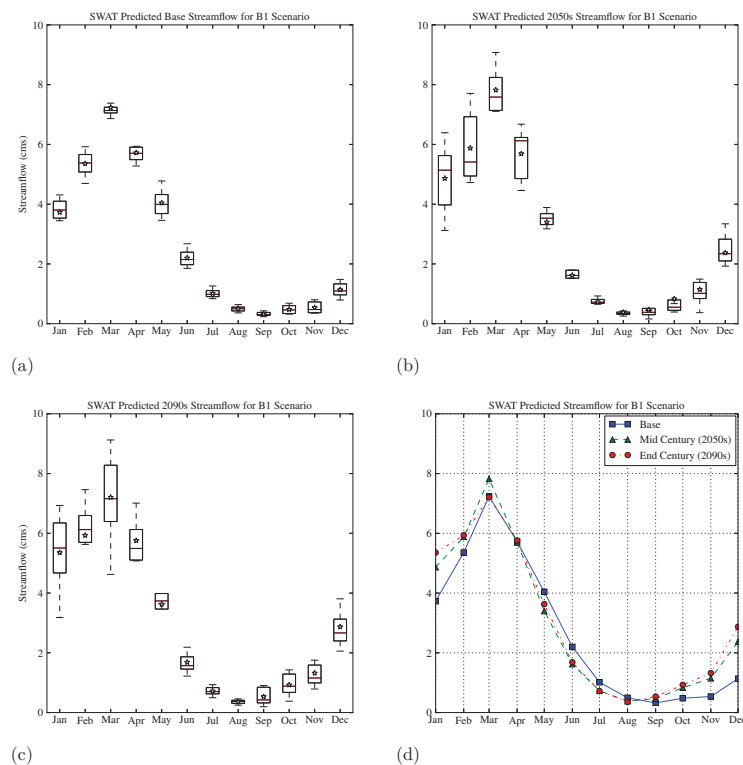


**Figure 6.** SWAT predicted monthly average streamflow. (a) Base period (1970–2000); (b) Mid-Century (2048–2065); (c) End-Century (2085–2099); from eight GCMs predicted B1 emission scenarios at USGS station 02085070; and, (d) the average streamflow over the eight GCMs for the three study periods.

### 3.3. Projected Changes in Nitrogen Transport

The SWAT simulation estimates an overall decrease of inorganic nitrogen loading by the mid-century and end century for both A2 and B1 scenarios. These decreases are  $-3.4\%$  ( $34.6$  to  $-44.9\%$ ) by the mid-century and  $-12.1\%$  ( $25.2$  to  $-53.4\%$ ) by the end century from the base condition ( $87.14 \text{ kg N d}^{-1}$ ) across the models for the A2 scenarios. For the B1 scenario, these decreases are  $-9.5\%$  ( $23.0$  to  $-25.5\%$ ) and  $-8.5\%$  ( $24.4$  to  $-32.5\%$ ), respectively. Individual model results also suggest a wider range of monthly average inorganic nitrogen values for the A2 scenario than the B1 scenario (Figures 7 and 8 and Table 3). Like streamflow, the variability in inorganic nitrogen loading can be explained by the seasonal changes and variability in the precipitation projections across the eight models (Table 2). For both A2 and B1 scenarios, the decreases are mainly in spring and summer months by  $-35.5\%$  ( $-17.8$  to  $-48.7\%$ ) and the increases are in fall and winter months by  $50.8\%$  ( $10.7$  to  $107.8\%$ ) by the end century (Table 4). Similar studies that were conducted in the Pike River watershed in southern Quebec [18] and the Eagle Creek Watershed in Indiana [21] using SWAT also predicted that nitrogen load would increase in winter and decrease in summer due to climate change.

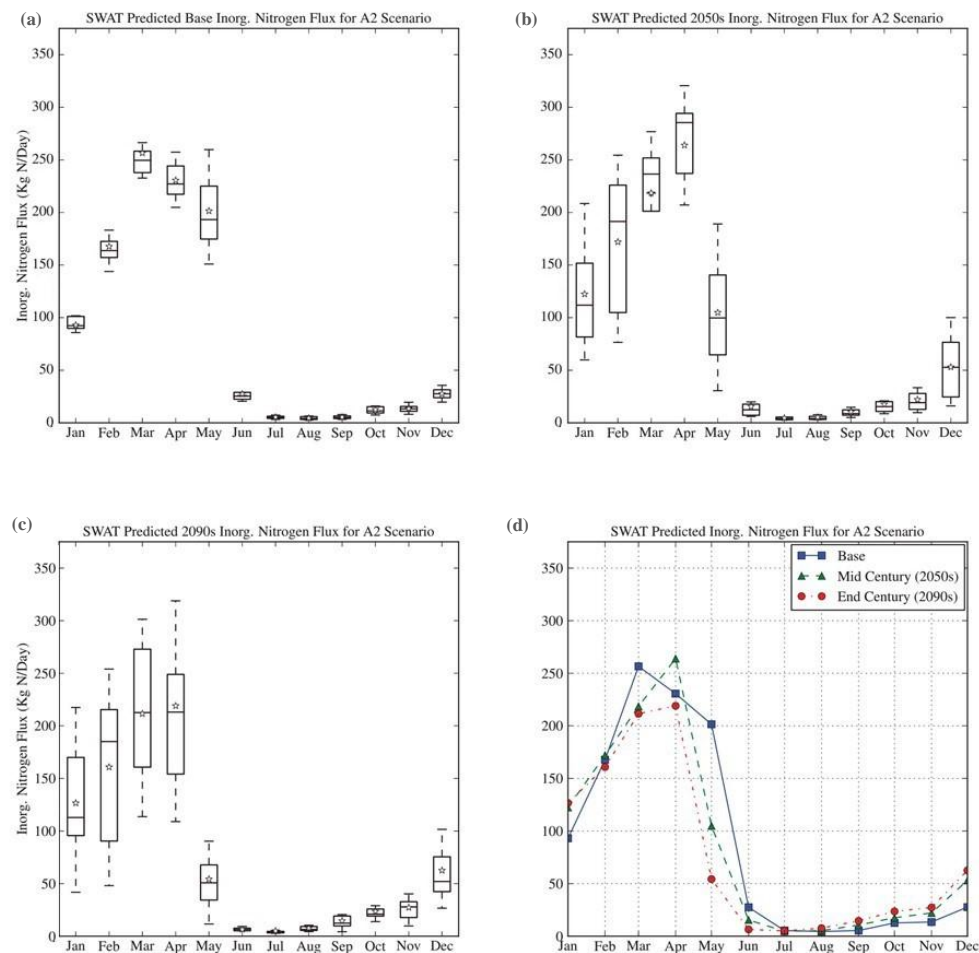


**Figure 7.** SWAT predicted monthly average inorganic nitrogen loading. (a) Base period (1970–2000); (b) Mid-Century (2048–2065); (c) End-Century (2085–2099); from eight GCMs predicted A2 emission scenarios at EPA station J0770000; and, (d) the average inorganic nitrogen loading over the eight GCMs for the three study periods.

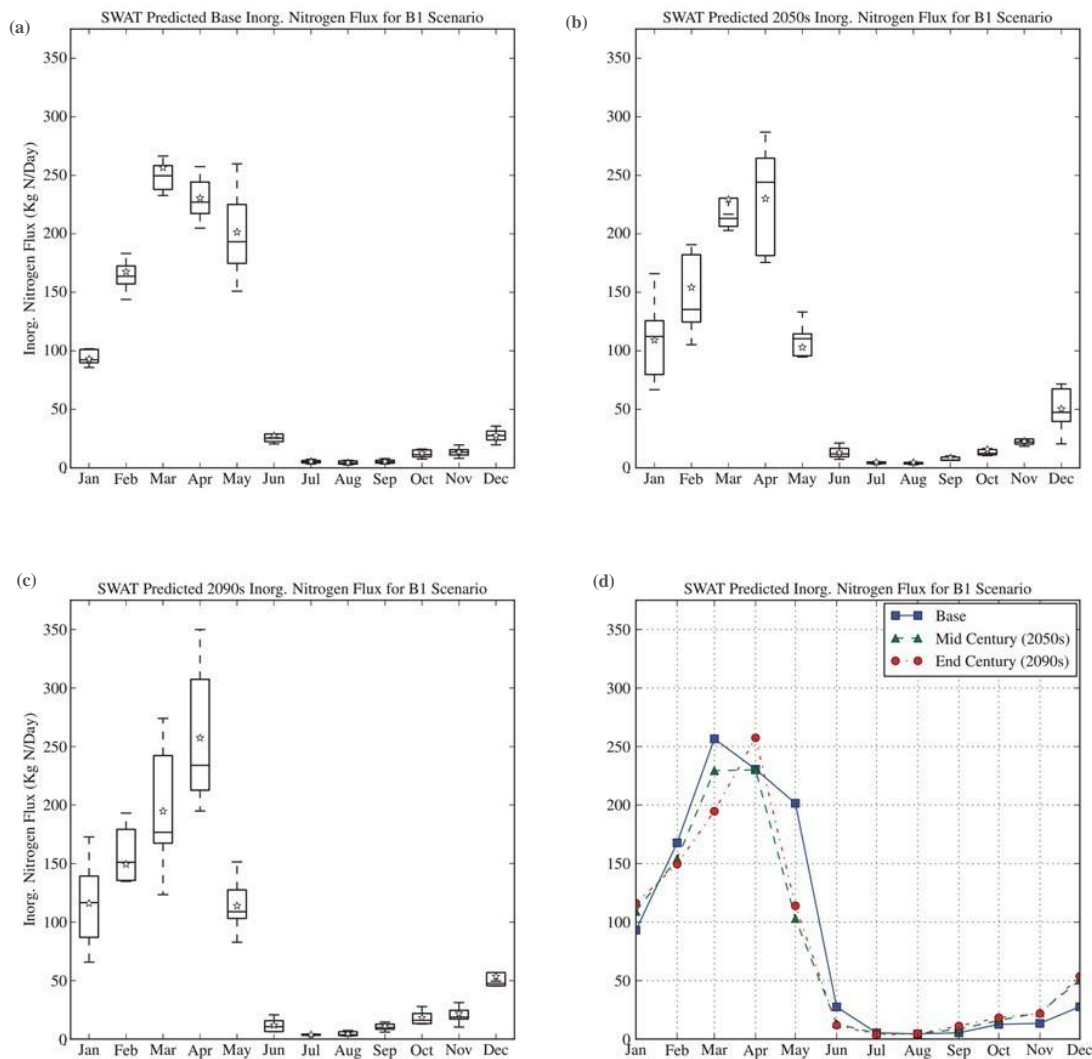


**Figure 8.** SWAT predicted monthly average inorganic nitrogen loading. (a) Base period (1970–2000); (b) Mid Century (2048–2065); (c) End Century (2085–2099); from eight GCMs predicted B1 emission scenarios at EPA station J0770000; and, (d) the average inorganic nitrogen loading over the eight GCMs for the three study periods.

#### 4. Discussion

The SWAT model parameterized using geospatial data layers of soil, topography and land use was used to investigate the impact of future climate (precipitation and temperature) alone on streamflow and nitrogen export for a small, forested watershed. A unique aspect of the study was the use of spatially downscaled GCM output from eight different GCMs to drive the hydrologic model. The results of the analysis suggest an overall increase in streamflow and decrease in inorganic nitrogen export over the century, but significant variability exists across GCMs. However, when viewed on a seasonal basis, there is more agreement across the models in terms of the general direction of streamflow and nitrogen export changes. Spring and summer months are projected to have lower streamflow and nitrogen export, while winter and fall months are expected to have higher streamflow and nitrogen export. A similar seasonal change in streamflow and nitrogen export due to climate change was found for Pike River watershed in southern Quebec that has similar land use, soil, and climate characteristics to our study watershed [18].

The ensemble of eight spatially downscaled GCMs for both the A2 and B1 scenarios shows general agreement in future temperature increases in the watershed. The precipitation projections, however,

vary widely with some models predicting an increase, while others predicting a decrease and the average across all models showing only a small increase of 0.8% and 1.5% for A2 and B1 scenarios, respectively, by the end century. Changes in both precipitation and temperature together result in an estimated increase in streamflow in the Eno River by, on average, 14.1% and 12.5%, respectively, for the A2 and B1 scenarios. This result is consistent with another study for two lowland catchments (Upper Narew and Barycz) in Poland with similar characteristics to the study watershed that also found water yield would increase due to projected temperature and precipitation changes [19].

This increase in streamflow is a result of the average increase in precipitation, but more so the seasonally disproportionate delivery of precipitation to the watershed that results in higher flows during the winter and fall seasons. More research is needed to further explore potential mechanistic reasons for the projected increase in streamflow that may also be due to changes in evapotranspiration rates that result in changes in soil moisture within the watershed. Soil moisture is a major factor in runoff response for watersheds and could be partially responsible for the model estimates of increase streamflow across the different model ensembles and emission scenarios. These interactions are complex and they require further study to fully explore.

The reduction in inorganic nitrogen export could be related to the increase of temperature across the GCMs. Many studies suggest a negative relationship between nitrogen loading and mean annual temperature increase [55–60]. The underlying mechanistic assumption is that temperature aids in denitrification processes [61–63], reducing the amount of fixed nitrogen and eventually decreasing nitrogen loading. This result was also found for another study while using the SWAT model for a semiarid Arizona watershed that also suggested a decrease in nitrate export due to climate change only [20].

Modeling nitrogen export within a physically-based watershed model remains a significant challenge. Uncertainty can arise from a variety of sources including a lack of quality in input data as well as the parameters selected to represent physical processes. On a daily time step, the streamflow model metrics suggested a reasonable predictive capability that is well within the range of previously published SWAT studies [29]. For our daily time step inorganic nitrogen calibration, due to limited nitrogen concentration observational data, the performance metrics for this nitrogen export calibration are lower than for streamflow, especially for  $R^2$ . Perhaps due to the complexity of modeling, inorganic nitrogen export at a watershed scale, we noted that most prior studies attempting to model nitrogen export did not report the  $R^2$  values of model predictions. Comparing to the available published model performance metrics and recommendation, especially in terms of percent bias ( $PB$ ), our calibration results can be considered to be satisfactory.

Future research should explore watersheds with more long term and high resolution inorganic nitrogen time series to increase confidence in the model predictions. In addition to improving the nitrogen observational record, the modeling performance could potentially be further improved by increasing the relatively short calibration and validation periods, or concentrating on only assessing models on seasonal or monthly time intervals. Past studies have shown that lower  $E$  values are typical for daily time step model runs [64] and short calibration and validation periods [65].

## 5. Conclusions

In summary, the results of this study suggest that climate change will result in increased streamflow and decreased inorganic nitrogen export over the twenty-first century for the study watershed. The high emission scenario (A2) and low emission scenario (B1) would result in an average increase in streamflow of 14.1% and 12.5%, respectively, by the end of the century. While changes in temperature are fairly consistent across the GCM models, changes in precipitation are highly variable, and this leads to significant uncertainty in the study results. Keeping this uncertainty in mind, the study results suggest that changes in precipitation along with changes in temperature will drive an overall decrease in inorganic nitrogen export for the study watershed. Inorganic nitrogen export is predicted to decrease by 12.1% and 8.5% for the A2 and B1 scenario, respectively, by the end of the

century. This decrease is believed to be a result of increases in temperature that result in increased denitrification and offset increases in nitrogen yield from the watershed that results from increased precipitation and streamflow. The studies conducted in the Pike River watershed in Québec and the Upper Narew and the Barycz catchments in Poland suggested increased streamflow and nitrogen export due to temperature and precipitation change. Although predicted streamflow agrees with our study result, nitrogen export disagrees, which may be explained by increased denitrification due to temperature increases. Another study for a semiarid watershed in Arizona also projected a decrease in nitrogen export. This speaks to the unique response of watersheds in different regions that may result from climate change.

Perhaps most significant is the seasonal variability in streamflow and nitrogen export found in the analysis. Both streamflow and nitrogen export are predicted to increase during the fall and winter months, but decrease in the spring and summer months. This can be explained by the variation in future seasonal precipitation that showed more consistency across the model ensemble. This result of seasonal changes in nitrogen export due to projected future climate conditions, with a significant increase in fall and winter months, will be important for water resource managers working to mitigate the impact of nitrogen pollution in waterbodies.

Finally, it is important to note that this study aims to understand how climate change alone may impact future nitrogen export within the study watershed. Other factors, such as development and nutrient mitigation strategies, will impact actual nitrogen export in the future. Understanding the potential impact of climate change alone can help to understand the influence of this potential stressor on future water quality conditions.

**Author Contributions:** M.J.A. and M.B.E. designed the methodology and analyzed the data; M.J.A. wrote the manuscript; J.L.G. acquired funding and supervised the study; F.T.Z. and J.L.G. reviewed and edited the manuscript.

**Funding:** The research was funded in part by the United States National Science Foundation (NSF) through award number CBET-0846244.

**Acknowledgments:** We acknowledge the modeling groups, the Program for Climate Model Diagnosis and Intercomparison (PCMDI) and the WCRP's Working Group on Coupled Modelling (WGCM) for their roles in making available the WCRP CMIP3 multi-model dataset.

**Conflicts of Interest:** The authors declare no conflict of interest.

## References

1. Cubasch, U.; Meehl, G.A.; Boer, G.J.; Stouffer, R.J.; Dix, M.; Noda, A.; Senior, C.A.; Raper, S.; Yap, K.S. The scientific basis. In *Contribution of Working Group I to the Third Assessment Report of the Intergovernmental Panel on Climate Change*; IPCC: Geneva, Switzerland, 2001.
2. Suddick, E.; Whitney, P.; Townsend, A.; Davidson, E. The role of nitrogen in climate change and the impacts of nitrogen—Climate interactions in the United States: Foreword to thematic issue. *Biogeochemistry* **2013**, *114*, 1–10. [[CrossRef](#)]
3. Lettenmaier, D.P.; Wood, E.F.; Wallis, J.R. Hydro—climatological trends in the continental United—States, 1948–88. *J. Clim.* **1994**, *7*, 586–607. [[CrossRef](#)]
4. Pachauri, R.K.; Reisinger, A. *Climate Change 2007: Synthesis Report; Contribution of Working Groups I, II and III to the Fourth Assessment Report of the Intergovernmental Panel on Climate Change*; The Intergovernmental Panel on Climate Change: Geneva, Switzerland, 2007.
5. Murdoch, P.S.; Baron, J.S.; Miller, T.L. Potential effects of climate change on surface—Water quality in North America. *J. Am. Water Resour. Assoc.* **2000**, *36*. [[CrossRef](#)]
6. Vitousek, P.M.; Aber, J.D.; Howarth, R.W.; Likens, G.E.; Matson, P.A.; Schindler, D.W.; Schlesinger, W.H.; Tilman, D.G. Human alteration of the global nitrogen cycle: Sources and consequences. *Ecol. Appl.* **1997**, *7*, 737–750. [[CrossRef](#)]
7. Hoagland, P.; Anderson, D.M.; Kaoru, Y.; White, A.W. The economic effects of harmful algal blooms in the United States: Estimates, assessment issues, and information needs. *Estuaries* **2002**, *25*, 819–837. [[CrossRef](#)]

8. Heisler, J.; Glibert, P.M.; Burkholder, J.M.; Anderson, D.M.; Cochlan, W.; Dennison, W.C.; Dortch, Q.; Gobler, C.J.; Heil, C.A.; Humphries, E.; et al. Eutrophication and harmful algal blooms: A scientific consensus. *Harmful Algae* **2008**, *8*, 3–13. [[CrossRef](#)] [[PubMed](#)]
9. US Environmental Protection Agency. *National Coastal Condition Report*; EPA-620/R-01/005; USEPA Office of Research and Development: Washington, DC, USA, 2001.
10. Morris, J.G., Jr. Harmful algal blooms: An emerging public health problem with possible links to human stress on the environment. *Annu. Rev. Energy Environ.* **1999**, *24*. [[CrossRef](#)]
11. Girvetz, E.H.; Zganjar, C.; Raber, G.T.; Maurer, E.P.; Kareiva, P.; Lawler, J.J. Applied climate—Change analysis: The climate Wizard tool. *PLoS ONE* **2009**, *4*. [[CrossRef](#)] [[PubMed](#)]
12. Arnold, J.G.; Srinivasan, R.; Muttiah, R.S.; Williams, J.R. Large area hydrologic modeling and assesment Part I: Model development. *JAWRA J. Am. Water Resour. Assoc.* **1998**, *34*, 73–89. [[CrossRef](#)]
13. Winchell, M.; Srinivasan, R.; Di Luzio, M.; Arnold, J.G. *ArcSWAT Interface For SWAT2012 User's Guide*; Blackland Research Center, Texas AgriLife Research: College Station, TX, USA, 2013.
14. Reichler, T.; Kim, J. How well do coupled models simulate today's climate. *Bull. Am. Meteorol. Soc.* **2008**, *89*, 303–311. [[CrossRef](#)]
15. Brekke, L.D.; Dettinger, M.D.; Maurer, E.P.; Anderson, M. Significance of model credibility in estimating climate projection distributions for regional hydroclimatological risk assessments. *Clim. Chang.* **2008**, *89*, 371–394. [[CrossRef](#)]
16. Pierce, D.W.; Barnett, T.P.; Santer, B.D.; Gleckler, P.J. Selecting global climate models for regional climate change studies. *Proc. Natl. Acad. Sci. USA* **2009**, *106*, 8441–8446. [[CrossRef](#)] [[PubMed](#)]
17. Maurer, E.P.; Brekke, L.; Pruitt, T.; Duffy, P.B. Fine—Resolution climate projections enhance regional climate change impact studies. *Eos Trans. Am. Geophys. Union* **2007**, *88*. [[CrossRef](#)]
18. Gombault, C.; Madramootoo, C.A.; Michaud, A.; Beaudin, I.; Sottile, M.-F.; Chikhaoui, M.; Ngwa, F. Impacts of climate change on nutrient losses from the Pike River watershed of southern Québec. *Can. J. Soil Sci.* **2015**. [[CrossRef](#)]
19. Marcinkowski, P.; Piniewski, M.; Kardel, I.; Szcześniak, M.; Benestad, R.; Srinivasan, R.; Ignar, S.; Okruszko, T. Effect of climate change on hydrology, sediment and nutrient losses in two lowland catchments in Poland. *Water* **2017**, *9*, 156. [[CrossRef](#)]
20. Ye, L.; Grimm, N.B. Modelling potential impacts of climate change on water and nitrate export from a mid—sized, semiarid watershed in the US Southwest. *Clim. Chang.* **2013**, *120*, 419–431. [[CrossRef](#)]
21. Ahmadi, M.; Records, R.; Arabi, M. Impact of climate change on diffuse pollutant fluxes at the watershed scale. *Hydrol. Process.* **2013**, *28*, 1962–1972. [[CrossRef](#)]
22. Praskievicz, S.; Chang, H. Impacts of climate change and urban development on water resources in the Tualatin River Basin, Oregon. *Ann. Assoc. Am. Geogr.* **2011**, *101*, 249–271. [[CrossRef](#)]
23. Pсарis, M.; Chang, H. Assessing the impacts of climate change, urbanization, and filter strips on water quality using SWAT. *Int. J. Geospatial Environ. Res.* **2014**, *1*, 1.
24. Gesch, D.; Oimoen, M.; Greenlee, S.; Nelson, C.; Steuck, M.; Tyler, D. The national elevation dataset. *Photogramm. Eng. Remote Sens.* **2002**, *68*, 5–11.
25. Fry, J.; Xian, G.; Jin, S.; Dewitz, J.; Homer, C.; Yang, L.; Barnes, C.; Herold, N.; Wickham, J. Completion of the 2006 national land cover database for the conterminous United States. *Photogramm. Eng. Remote Sens.* **2006**, *77*, 858–864.
26. Larose, M.; Heathman, G.C.; Norton, L.D.; Engel, B. Hydrologic and atrazine simulation of the cedar creek watershed using the SWAT model. *J. Environ. Qual.* **2007**, *36*, 521. [[CrossRef](#)] [[PubMed](#)]
27. Ercan, M.B.; Goodall, J.L. Estimating watershed—Scale precipitation by combining gauge—and radar—derived observations. *J. Hydrol. Eng.* **2012**, *18*, 983–994. [[CrossRef](#)]
28. Runkel, R.L.; Crawford, C.G.; Cohn, T.A. *Load Estimator (Loadest): A Fortran Program for Estimating Constituent Loads in Streams and Rivers*; U.S. Geological Survey: Reston, VA, USA, 2004.
29. Gassman, P.W.; Reyes, M.R.; Green, C.H.; Arnold, J.G. *The Soil and Water Assessment Tool: Historical Development, Applications, and Future Research Directions*; Center for Agricultural and Rural Development, Iowa State University: Ames, IA, USA, 2007.
30. U.S. Environmental Protection Agency. *Protocol for Developing Pathogen TMDLs First Edition*; U.S. Environmental Protection Agency: Washington, DC, USA, 1999.

31. Rallison, R.E.; Miller, N. Past, present, and future SCS runoff procedure. In *Proceedings of the International Symposium on Rainfall-Runoff Modeling, 18–21 May 1981*; Singh, V.P., Ed.; Mississippi State University: Starkville, MS, USA, 1982.
32. Allen, R.G. A penman for all seasons. *J. Irrig. Drain. Eng.* **1986**, *112*, 348–368. [[CrossRef](#)]
33. Williams, J.R. Flood routing with variable travel time or variable storage coefficients. *Trans. ASAE* **1969**, *12*, 100–103. [[CrossRef](#)]
34. McElroy, A.D. *Loading Functions for Assessment of Water Pollution from Nonpoint Sources*; US Environmental Protection Agency, Office of Research and Development, Office of Air, Land, and Water Use: Washington, DC, USA, 1976.
35. Williams, J.R.; Hann, R.W. *Optimal Operation of Large Agricultural Watersheds with Water Quality Restraints*; Texas Water Resources Institute: College Station, TX, USA, 1978.
36. Neitsch, S.L.; Arnold, J.G.; Kiniry, J.R.; Williams, J.R. Soil and Water Assessment Tool User’s Manual Version 2005. *Diffus. Pollut. Conf. Dublin* **2005**, 494.
37. Meehl, G.A.; Covey, C.; Delworth, T.; Latif, M.; McAvaney, B.; Mitchell, J.F.B.; Stouffer, R.J.; Taylor, K.E. The WCRP CMIP3 multimodel dataset: A new era in climatic change research. *Bull. Am. Meteorol. Soc.* **2007**, *88*, 1383–1394. [[CrossRef](#)]
38. Baker, N.C.; Huang, H.P. A comparative study of precipitation and evaporation between CMIP3 and CMIP5 climate model ensembles in semiarid regions. *J. Clim.* **2014**, *27*, 3731–3749. [[CrossRef](#)]
39. Sun, Q.; Miao, C.; Duan, Q. Comparative analysis of CMIP3 and CMIP5 global climate models for simulating the daily mean, maximum, and minimum temperatures and daily precipitation over China. *J. Geophys. Res.* **2015**, *120*, 4806–4824. [[CrossRef](#)]
40. Flato, G.M.; Boer, G.J. Warming asymmetry in climate change simulations. *Geophys. Res. Lett.* **2001**, *28*, 195–198. [[CrossRef](#)]
41. Salas–Mélia, D.; Chauvin, F.; Déqué, M.; Douville, H.; Gueremy, J.; Marquet, P.; Planton, S.; Royer, J.; Tyteca, S. Description and validation of the CNRM-CM3 global coupled model. *Clim. Dyn.* **2005**, 103.
42. Delworth, T.L.; Broccoli, A.J.; Rosati, A.; Stouffer, R.J.; Balaji, V.; Beesley, J.A.; Cooke, W.F.; Dixon, K.W.; Dunne, J.; Dunne, K.A.; et al. GFDL’s CM2 global coupled climate models. Part I: Formulation and simulation characteristics. *J. Clim.* **2006**, *19*, 643–674. [[CrossRef](#)]
43. Marti, O.; Braconnot, P.; Bellier, J.; Benshila, R.; Bony, S.; Brockmann, P.; Cadule, P.; Caubel, A.; Denvil, S.; Dufresne, J.-L.; et al. *The New IPSL Climate System Model: IPSL–CM4*; Institut Pierre–Simon Laplace (IPSL): Paris, France, 2006.
44. Hasumi, H.; Emori, S. *K-1 Coupled GCM (MIROC) Description. K-1 Technical Report, 1. K-1 Model Developers*; Center for Climate System Research. University of Tokyo: Tokyo, Japan, 2004.
45. Legutke, S.; Voss, R. *The Hamburg Atmosphere–Ocean Coupled Circulation Model-ECHO-G*; DKRZ Technical Report No. 18; German Climate Computer Center: Hamburg, Germany, 1999.
46. Jungclaus, J.H.; Keenlyside, N.; Botzet, M.; Haak, H.; Luo, J.J.; Latif, M.; Marotzke, J.; Mikolajewicz, U.; Roeckner, E. Ocean circulation and tropical variability in the coupled model ECHAM5/MPI–OM. *J. Clim.* **2006**, *19*, 3952–3972. [[CrossRef](#)]
47. Yukimoto, S.; Noda, A.; Kitoh, A.; Sugi, M.; Kitamura, Y.; Hosaka, M.; Shibata, K.; Maeda, S.; Uchiyama, T. The new meteorological research institute coupled GCM (MRI-CGCM2). Model climate and variability. *Pap. Meteorol. Geophys.* **2001**, *51*, 47–88. [[CrossRef](#)]
48. Gates, W.L. The use of general circulation models in the analysis of the ecosystem impacts of climatic change. *Clim. Chang.* **1985**, *7*, 267–284. [[CrossRef](#)]
49. Beven, K.; Binley, A. The future of distributed models: Model calibration and uncertainty prediction. *Hydrol. Process.* **1992**, *6*, 279–298. [[CrossRef](#)]
50. Abbaspour, K.C. *SWAT–CUP 2012: SWAT Calibration and Uncertainty Programs—A User Manual*; Eawag Swiss Federal Institute Aquatic Science and Technology: Dübendorf, Switzerland, 2012.
51. Andersen, J.; Refsgaard, J.C.; Jensen, K.H. Distributed hydrological modelling of the Senegal River Basin—model construction and validation. *J. Hydrol.* **2001**, *247*, 200–214. [[CrossRef](#)]
52. Deb, K.; Pratab, S.; Agarwal, S.; Meyarivan, T. A fast and elitist multiobjective genetic algorithm: NSGA–II. *IEEE Trans. Evol. Comput.* **2002**, *6*, 182–197. [[CrossRef](#)]
53. Ercan, M.B.; Goodall, J.L. Design and implementation of a general software library for using NSGA–II with SWAT for multi–objective model calibration. *Environ. Model. Softw.* **2016**, *84*, 112–120. [[CrossRef](#)]

54. Moriasi, D.N.; Arnold, J.G.; Van Liew, M.W.; Bingner, R.L.; Harmel, R.D.; Veith, T.L. Model evaluation guidelines for systematic quantification of accuracy in watershed simulations. *Trans. ASABE* **2007**, *50*, 885–900. [[CrossRef](#)]
55. Alexander, R.B.; Smith, R.A.; Schwarz, G.E.; Boyer, E.W.; Nolan, J.V.; Brakebill, J.W. Differences in phosphorus and nitrogen delivery to the Gulf of Mexico from the Mississippi River Basin. *Environ. Sci. Technol.* **2008**, *42*, 822–830. [[CrossRef](#)] [[PubMed](#)]
56. Najjar, R.G.; Pyke, C.R.; Adams, M.B.; Breitburg, D.; Hershner, C.; Kemp, M.; Howarth, R.; Mulholland, M.R.; Paolisso, M.; Secor, D.; et al. Potential climate—Change impacts on the Chesapeake Bay. *Estuar. Coast. Shelf. Sci.* **2010**, *86*, 1–20. [[CrossRef](#)]
57. Rebich, R.A.; Houston, N.A.; Mize, S.V.; Pearson, D.K.; Ging, P.B.; Evan Hornig, C. Sources and delivery of nutrients to the northwestern gulf of Mexico from streams in the south-central United States. *JAWRA J. Am. Water Resour. Assoc.* **2011**, *47*, 1061–1086. [[CrossRef](#)] [[PubMed](#)]
58. Wise, D.R.; Johnson, H.M. Surface-water nutrient conditions and sources in the United States Pacific Northwest. *JAWRA J. Am. Water Resour. Assoc.* **2011**, *47*, 1110–1135. [[CrossRef](#)] [[PubMed](#)]
59. Alam, M.J.; Goodall, J.L. Toward disentangling the effect of hydrologic and nitrogen source changes from 1992 to 2001 on incremental nitrogen yield in the contiguous United States. *Water Resour. Res.* **2012**, *48*. [[CrossRef](#)]
60. Alam, M.J.; Goodall, J.L.; Bowes, B.D.; Girvetz, E.H. The impact of projected climate change scenarios on nitrogen yield at a regional scale for the contiguous United States. *J. Am. Water Resour. Assoc.* **2017**, *53*, 854–870. [[CrossRef](#)]
61. Seitzinger, S.P. Denitrification in freshwater and coastal marine ecosystems: Ecological and geochemical significance. *Limnol. Oceanogr.* **1988**, *33*, 702–724. [[CrossRef](#)]
62. Veraart, A.J.; de Klein, J.J.M.; Scheffer, M. Warming can boost denitrification disproportionately due to altered oxygen dynamics. *PLoS ONE* **2011**, *6*. [[CrossRef](#)] [[PubMed](#)]
63. Jha, M.K.; Gassman, P.W.; Panagopoulos, Y. Regional changes in nitrate loadings in the Upper Mississippi River Basin under predicted mid-century climate. *Reg. Environ. Chang.* **2013**, *15*, 449–460. [[CrossRef](#)]
64. Grizzetti, B.; Bouraoui, F.; De Marsily, G. Modelling nitrogen pressure in river basins: A comparison between a statistical approach and the physically-based SWAT model. *Phys. Chem. Earth Parts A/B/C* **2005**, *30*, 508–517. [[CrossRef](#)]
65. Muleta, M.K.; Nicklow, J.W. Sensitivity and uncertainty analysis coupled with automatic calibration for a distributed watershed model. *J. Hydrol.* **2005**, *306*, 127–145. [[CrossRef](#)]



© 2018 by the authors. Licensee MDPI, Basel, Switzerland. This article is an open access article distributed under the terms and conditions of the Creative Commons Attribution (CC BY) license (<http://creativecommons.org/licenses/by/4.0/>).